Metallicity beats sSFR: the connection between superluminous supernova host galaxy environments and the importance of metallicity for their production

Cleland, Cressida; Mcgee, Sean L; Nicholl, Matt

DOI:
10.1093/mnras/stad2118

Document Version
Publisher's PDF, also known as Version of record

Citation for published version (Harvard):
Cleland, C, Mcgee, SL & Nicholl, M 2023, 'Metallicity beats sSFR: the connection between superluminous supernova host galaxy environments and the importance of metallicity for their production', *Monthly Notices of the Royal Astronomical Society*, vol. 524, no. 3, pp. 3559-3567. https://doi.org/10.1093/mnras/stad2118

Monthly Notices of the ROYAL ASTRONOMICAL SOCIETY

MNRAS **524,** 3559–3567 (2023) https://doi.org/10.1093/mnras/stad2118
Advance Access publication 2023 July 14

Metallicity beats sSFR: the connection between superluminous supernova host galaxy environments and the importance of metallicity for their production

Cressida Cleland,[1]★ Sean L. McGee[1] and Matt Nicholl[2]

[1]*School of Physics and Astronomy, University of Birmingham, Edgbaston, Birmingham B15 2TT, UK*
[2]*Astrophysics Research Centre, School of Mathematics and Physics, Queen's University Belfast, Belfast BT7 1NN, UK*

Accepted 2023 July 12. Received 2023 July 12; in original form 2023 January 25

ABSTRACT

We analyse 33 Type I superluminous supernovae (SLSNe) taken from Zwicky Transient Facility (ZTF)'s Bright Transient Survey to investigate the local environments of their host galaxies. We use a spectroscopic sample of galaxies from the Sloan Digital Sky Survey (SDSS) to determine the large-scale environmental density of the host galaxy. Noting that SLSNe are generally found in galaxies with low stellar masses, high star formation rates (SFRs), and low metallicities, we find that SLSN hosts are also rarely found within high-density environments. Only 3^{+9}_{-1} per cent of SLSN hosts were found in regions with two or more bright galaxies within 2 Mpc. For comparison, we generate a sample of 662 SDSS galaxies matched to the photometric properties of the SLSN hosts. This sample is also rarely found within high-density environments, suggesting that galaxies with properties required for SLSN production favour more isolated environments. Furthermore, we select galaxies within the IllustrisTNG simulation to match SLSN host galaxy properties in colour and stellar mass. We find that the fraction of simulated galaxies in high-density environments quantitatively match the observed SLSN hosts only if we restrict to simulated galaxies with metallicity $12 + \log(\mathrm{O/H}) \leq 8.12$. In contrast, limiting to only the highest specific star formation rate (sSFR) galaxies in the sample leads to an overabundance of SLSN hosts in high-density environments. Thus, our measurement of the environmental density of SLSN host galaxies appears to break the degeneracy between low metallicity and high sSFR as the driver for SLSN hosts and provides evidence that the most constraining factor on SLSN production is low metallicity.

Key words: galaxies: evolution – galaxies: star formation – transients: supernovae.

1 INTRODUCTION

While the detection rates of supernovae (SNe) have rapidly increased over the last decade or so, thanks to wide-field high-cadence surveys such as the Panoramic Survey Telescope and Rapid Response System (Pan-STARRS; Chambers et al. 2016), Asteroid Terrestrial-impact Last Alert System (ATLAS; Tonry et al. 2018), and Zwicky Transient Facility (ZTF; Bellm et al. 2019), superluminous supernovae (SLSNe) remain a rare and elusive transient event. SLSNe were originally classed as a supernova (SN) event that is 10–100 times brighter than typical SNe (Quimby et al. 2011; Gal-Yam 2012), however are now classified by their unique spectra (e.g. Lunnan et al. 2018; Quimby et al. 2018; Angus et al. 2019). Their light curves differ from those of other SNe as they are both broader and brighter. There are two classes of SLSNe: Type I and Type II. Type I SLSNe (often referred to as simply SLSNe, a convention we adopt in this work) are dominated by O II absorption lines at maximum luminosity, while Type II SLSNe exhibit sharply peaked hydrogen emission lines from circumstellar interaction. The physical mechanisms that cause Type I SLSNe remain a topic of debate, with mechanisms such as a central engine in the form of a magnetar (see e.g. Kasen & Bildsten 2010; Inserra et al. 2013; Nicholl, Guillochon & Berger 2017) or interaction with the circumstellar medium (see e.g. Smith & McCray 2007; Chevalier & Irwin 2011; Chatzopoulos, Wheeler & Vinko 2012; Ginzburg & Balberg 2012) being proposed as possible power sources for the increased luminosity.

We can use properties of their host galaxies to infer the conditions required for a SLSN to occur. This can help constrain the processes at work. SLSNe have been found mostly in low-mass galaxies, with very few being found in host galaxies with stellar mass $>10^8$ $\mathrm{M}_\odot$ (Schulze et al. 2018). This is surprising, as one might expect that with more stars come more SN events (Sullivan et al. 2006; Smith et al. 2012; Wiseman et al. 2021, see also Perley et al. 2016a). Various authors have found that SLSN host galaxies typically have high specific star formation rates (sSFRs, $\sim 10^{-9}$ yr^{-1}; Neill et al. 2011; Leloudas et al. 2015; Angus et al. 2016), leading to the idea that SLSNe may be the first stars to explode following a starburst. Leloudas et al. (2015) note that SLSN host galaxies have properties that are consistent with extreme emission line galaxies (EELGs), i.e. high sSFR and also highly ionized gas. Meanwhile, Lunnan et al. (2014), Chen et al. (2017), and Perley et al. (2016b) argue that the low metallicity observed in SLSN hosts is the more important factor in the production of these rare transients, and that their low metallicities can explain the extreme energies seen (Chen et al. 2013). Nevertheless, since dwarf galaxies tend to have both low metallicities and bursty

★ E-mail: cressidac@star.sr.bham.ac.uk

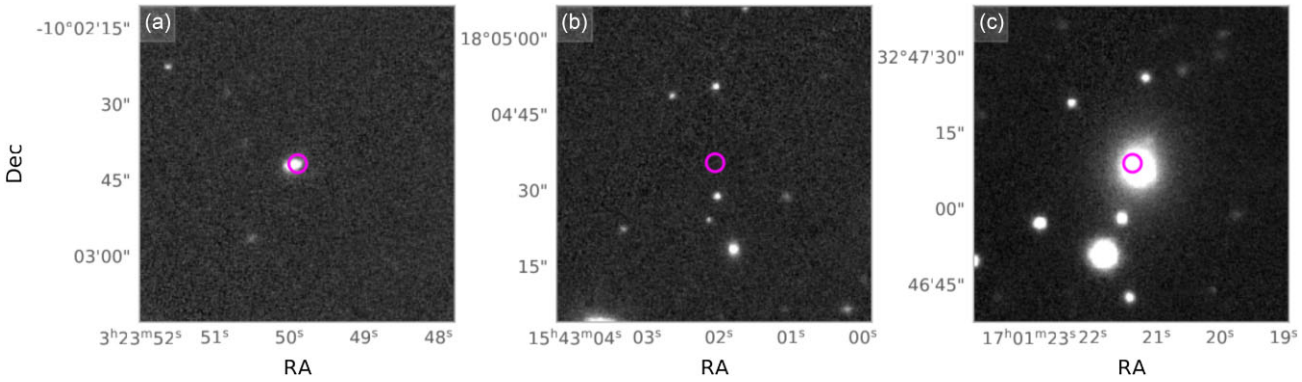

Figure 1. PanSTARRS *i*-band cutout images (Flewelling et al. 2020) of SLSN sources and of a Type Ia SN host. Panel (a) shows object ZTF21aaarmti, panel (b) shows object ZTF22aalzjdc, and panel (c) shows object ZTF18aangpkx. The magenta circle in each panel depicts the location of the source. In panel (b), no host galaxy was found for the source. The host galaxy in panel (c) is in a higher density environment than the SLSN hosts; see Section 3.1 for details. The absolute magnitude of the host galaxy in panel (a) is $M_i = -21.36$ and its redshift is $z = 0.193$. The absolute magnitude of the host galaxy in panel (c) is $M_i = -22.67$ and its redshift is $z = 0.070$. The redshift of the SLSN source in panel (b) is $z = 0.200$. The size of each of the images is 62.50 arcsec.

star formation histories, and the production of SLSNe appears averse to high metallicity and low sSFR (Schulze et al. 2018), there is a degeneracy regarding which of these factors is more critical.

It is well known that the local environment of galaxies, i.e. whether a galaxy is located within a galaxy group or a galaxy cluster or it is isolated, has a profound effect on a number of galaxy properties, including the metallicity (Tremonti et al. 2004; Cooper, Newman & Yan 2009; Ellison et al. 2009), star formation rate (SFR; Wetzel et al. 2013; Cleland & McGee 2021), and overall evolution of the galaxy (Dressler 1980). Gravitational interactions between galaxies can disturb the gas and dust that fuel star formation, leading to starburst phases, or similarly galaxies may merge that will also have an effect on the SFRs of the galaxies involved. Conversely, high-density environments may cause the quenching of star formation in an infalling galaxy. It naturally follows to investigate the local environment of SLSNe host galaxies to uncover any environmental factors that may impact SLSNe rates. Ørum et al. (2020) find that up to 50 per cent of SLSN host galaxies have at least one companion within 5 kpc, which they use to explain the increased SFRs required for SLSNe to occur. However, for the purposes of this work we are interested in the overall density of the local environment of the SLSN host galaxy. That is, a close companion galaxy of arbitrary stellar mass within kpc of the SN host galaxy does not necessarily lead to the same environmental effects at larger scales (e.g. Mpc). In order to probe for such effects, we aim to use bright galaxies as a proxy for density, noting that this is a first-order approach, with the absolute magnitude of galaxies roughly tracing stellar mass. By investigating the environments of these galaxies in this way, we aim to break the degeneracy between the requirements of low metallicity and high sSFR for SLSN production.

In this work, we identify isolated SLSNe and SLSNe in groups, and compare between various host galaxy properties. We also compare against Type Ia SN host galaxies, which occur in a wider variety of host galaxies. We then investigate these host galaxies further within the IllustrisTNG simulation suite, by exploring the metallicities and sSFRs of a sample of simulated galaxies with observational properties similar to those of SLSN hosts.

The paper is structured as follows. In Section 2, we describe the data used and how it were obtained. In Section 3, we explain the results and discuss their implications. Finally, in Section 4, we summarize our findings. For the computation of cosmological distances, we use a flat Universe with $H_0 = 70.2$ and $\Omega_m = 0.277$.

2 DATA

We obtain coordinates, redshifts, and host photometry ($g - i$ colours and M_i absolute magnitudes) of 55 Type I SLSNe (hereafter simply referred to as SLSNe) and 4816 Type Ia SNe from the ZTF Bright Transient Survey[1] (BTS; Masci et al. 2019; Perley et al. 2020a). This was the full sample of SLSNe and Type Ia SNe available on the BTS at the time of analysis (2022 September). The BTS is used to obtain properties on SN events and their host galaxies due it being a well-defined sample with a limiting magnitude of ≈18.5 mag that selects for nearby events with a higher chance of host detection. The SNe in this sample have been classified spectroscopically, and by a variety of research groups. Table A1 lists and cites the classification group for each SLSN. The code SHERLOCK[2] is used to cross-identify for a host galaxy and its photometry (Smith et al. 2020); this information is available directly on the LASAIR broker (Smith et al. 2019) for each source. Some sources have no catalogued host, and are marked as 'orphans'. See Fig. 1 for examples of a SLSN source with a host detection (left-hand panel) and a SLSN source where no host was detected (middle panel). We denote the SLSN host galaxy sample as SLSN-g, and the Type Ia SN host galaxy sample as SN-Ia.

We obtain a spectroscopically redshifted sample of 300 000 random galaxies (Spec-z) from the Sloan Digital Sky Survey (SDSS) Data Release 17 (DR17; Smee et al. 2013; Blanton et al. 2017; Abdurro'uf et al. 2022), such that their redshifts are local and precisely known, $0 < z < 0.4$. We also obtain 16 494 random photometrically redshifted galaxies from SDSS DR17 (Fukugita et al. 1996; Gunn et al. 1998, 2006; Doi et al. 2010) to better match the parameter space of the SLSNe sample, with $0 < z < 0.4$, such that $z_{err} < 0.1$ and $z_{err}/z < 0.5$. Both samples were obtained using the SDSS query service CasJobs.[3] For each sample of SN hosts, we restrict to sources within the on-sky footprint of the spectroscopic sample, resulting in 35 SLSNe (18 with detected hosts) and 3450 Type Ia SNe.

[1] https://sites.astro.caltech.edu/ztf/bts/bts.php
[2] https://github.com/thespacedoctor/sherlock
[3] http://cas.sdss.org/dr17/

Table 1. Descriptions of each of the samples used. The ranges shown in the redshift and magnitude columns refer to the minima and maxima of that property for each sample, not necessarily the selection constraints.

Sample	# obj.	Redshift	Median (z)	Magnitude	Median (M_i)	Description
SLSN-g	33	$0.064 \leq z \leq 0.39$	0.159	$-22.74 \leq M_i \leq -15.32$	-18.41	SLSN host galaxies
SDSS-m	662	$0.036 \leq z \leq 0.312$	0.117	$-22.196 \leq M_i \leq -16.709$	-19.632	SDSS photometric-z galaxies matched to SLSN-g
SN-Ia	3268	$0.001 \leq z \leq 0.0.156$	0.065	$-26.56 \leq M_i \leq -11.56$	-20.76	Type Ia SN host galaxies
Spec-z	300 000	$0.0 \leq z \leq 0.4$	0.144	$-31.214 \leq M_i \leq -10.006$	-22.385	SDSS spectroscopic-z galaxies

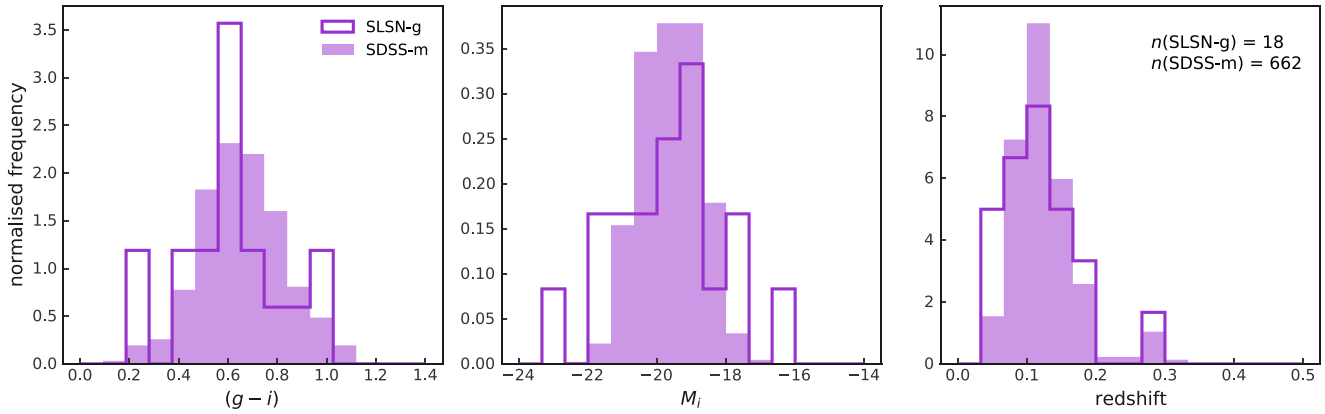

Figure 2. Histograms of the colours, absolute magnitudes, and redshifts of galaxies in SLSN-g with reliable photometry compared to the matched SDSS sample. KS tests result in p-values of 0.46, 0.36, and 0.75, respectively, validating that the SLSN-g and SDSS-m samples match each other.

2.1 Matched sample generation

Since the number of SLSN host galaxies is so low, it is desirable to generate a matched galaxy sample, based on SLSN host galaxy properties. This means we can make statistical comparisons of SLSN host-like galaxies, but on a much larger sample of galaxies. The properties of the SLSN host galaxies are based on their photometry, so we generate a sample of galaxies that are matched based on photometric properties such as absolute magnitude and colour. We generate this matched sample to the SLSN host galaxies from the SDSS photometric galaxies (Cooper et al. 2009). For each SLSN host galaxy, we randomly search for a photometric galaxy within a sphere in parameter space according to equation (1):

$$\left(\frac{\Delta\,\text{colour}}{0.2}\right)^2 + \left(\frac{\Delta M_i}{1.2}\right)^2 + \left(\frac{\Delta z}{0.04}\right)^2 = 1, \quad (1)$$

where Δ colour, ΔM_i, and Δz refer to the difference between the $(g-i)$ colour, absolute magnitude, and redshift of the SLSN host galaxy and the photometric galaxy. The scaling factor in the denominator of each term in equation (1) comes from taking the range of each property and multiplying by a factor of 0.1. This factor was chosen by visual inspection to ensure an adequate chance of finding an appropriate match, while reducing mismatches in parameter space. Applying this factor ensures each property has the same weight in parameter space. We attempt a random search for a unique SDSS galaxy that satisfies equation (1) on a SLSN host galaxy; this search gets repeated until a match is found, to a maximum of 1000 times. This process is repeated on SLSN host galaxies 10 000 times. This results in a matched sample (SDSS-m) of 662 galaxies. Note that varying the multiplicative factor in equation (1), and the number of repetitions performed on each galaxy, has no quantitative effect on the results discussed in Section 3.1. For this matching procedure, we only use the 18 SLSN sources with detected hosts and reliable host photometry. The rest of the analysis depends on the positions and redshifts of each SLSN source directly, and so the entire sample of 33 SLSNe is used.

The details of each sample are listed in Table 1. Histograms of the distributions of the colour, absolute magnitude, and redshift of SLSN-g and SDSS-m are plotted in Fig. 2. Kolmogorov–Smirnov (KS) tests validate that the distributions match well, with the added benefit of over an order of magnitude more galaxies in the matched sample than SLSN host galaxies.

3 RESULTS AND DISCUSSION

3.1 Observations

Using bright, well-observed galaxies as a proxy for density, we count the number of bright ($M_i < -21.5$) Spec-z galaxies that are at an on-sky projection of 2 Mpc or less of the target galaxy, within $\Delta z = 0.005$, based on a typical velocity dispersion of a galaxy group/cluster (Yang et al. 2007). We denote this quantity as N_2. We use $M_i < -21.5$ as the threshold for bright galaxies as this magnitude is the completion limit for the entire spectroscopic sample for this redshift range, and we use 2 Mpc as it is the upper end of galaxy group diameters (Yang et al. 2007). Note that varying the M_i threshold does not have a qualitative effect on the results. We calculate N_2 for SLSN-g, SDSS-m, and SN-Ia as a control. SN-Ia works as a control sample because these galaxies are much less confined to a specific region of parameter space compared to SLSNe, and the photometry is easily comparable to SLSN-g since both samples come from ZTF. A two-dimensional (2D) histogram showing these results is shown in Fig. 3, with N_2 shown as a function of absolute magnitude. Note the log scale in the z-axis. This quantity is also plotted for SLSN-g and SDSS-m in dark purple and light purple, respectively. We can see that while the distribution N_2 for SN-Ia occupies a large and varied region of parameter space (note 70 per cent of SN-Ia still has $N_2 = 0$), $N_2 \leq 2$ for SLSN-g and $N_2 \leq 3$ for SDSS-m, with the majority of

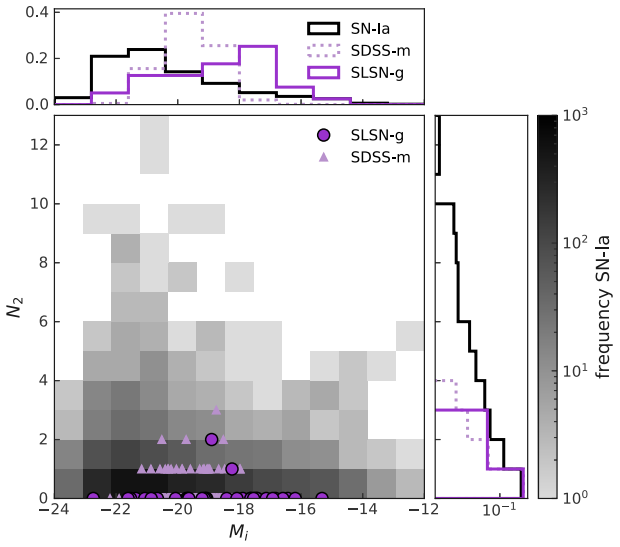

Figure 3. A scatter plot of the number of bright Spec-z galaxies within 2 Mpc of a target galaxy against absolute magnitude, compared to a 2D histogram of the same distribution for Type Ia SNe host galaxies. SLSN-g is shown as dark purple circles and the matched sample, SDSS-m, is shown as light purple triangles. Normalized histograms are included on the x and y axes and show the absolute magnitude and N_2 distributions for SN-Ia, SDSS-m, and SDSS-g.

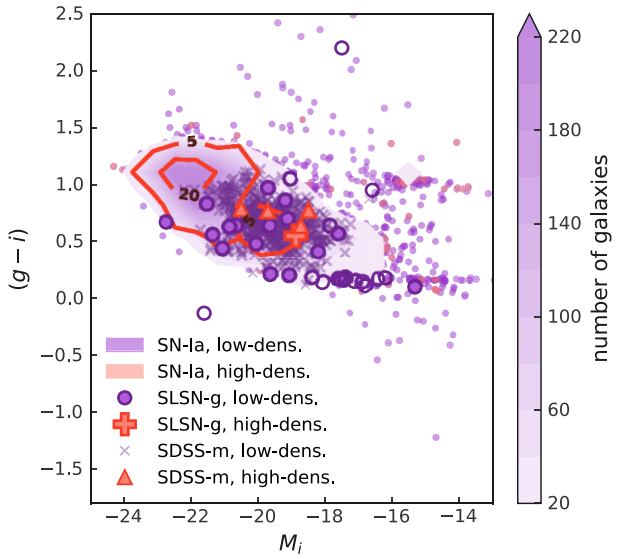

Figure 4. A colour–magnitude diagram comparing SLSN-g and SDSS-m to SN-Ia. Low-density SLSN-g galaxies are plotted in purple circles, high-density SLSN-g galaxies are plotted in orange pluses, low-density SDSS-m galaxies are plotted in purple crosses, high-density SDSS-m are plotted in orange triangles, and the distributions for low- and high-density SN-Ia galaxies are plotted as purple filled in contours and orange contour lines, respectively. Open purple circles represent the SLSN-g sources with unreliable host photometry. Purple and orange points shown individual SN-Ia galaxies when they are not captured by the contours.

galaxies having $N_2 = 0$. This is not simply a consequence of reduced numbers of SLSN-g compared to SN-Ia; binned by magnitude, the fraction of SLSN-g with any bright neighbour (i.e. $N_2 \geq 1$) reaches a maximum of about 10 per cent,[4] which is only half of the minimum of the fraction of SN-Ia with any neighbour in the same bins. Similarly, SDSS-m only reaches a maximum of about 10 per cent.

We consider galaxies with $N_2 \geq 2$ as being in a high-density environment, with everything else being in a low-density environment. This number is chosen under the assumption that a typical galaxy group or cluster halo is of the order of a few Mpc in diameter (Yang et al. 2007), so any more than two bright (large) galaxies would be considered a high-density environment. We emphasize the fact that this is a generous constraint, set in an attempt to maximize the number of SLSN hosts in high-density environments. An example of a SN-Ia host galaxy with a high N_2 number ($N_2 = 8$) is shown in the right-hand panel of Fig. 1. We plot SLSN-g, SDSS-m, and SN-Ia on a colour–magnitude diagram in Fig. 4, separated by high and low density. Contour lines map out the SN-Ia galaxies that are in high-density environments. We see that the high-density SLSN-g and SDSS-m galaxies are found on the outer regions of these contour lines. That is, they preferentially avoid the region in phase space where high-density environments occur. This result, along with finding that the matched sample galaxies are also almost exclusively found in low-density environments, is indicative that the galactic properties of SLSN hosts are the constraining factor in the density of the environment of these galaxies. In other words, the types of galaxies where SLSNe are found (blue low mass and low metallicity) are rarely found in high-density environments. As a fraction of each sample, SLSNe that occur in high-density environments are at $1/33 = 0.03\pm^{0.06}_{0.01}$, and matched galaxies that occur in high-density environments are even lower, at $4/662 = 0.006\pm^{0.005}_{0.002}$.

[4]This number is entirely dependent on the choice of binning since $N_2 \approx 1$ for SLSN-g in any magnitude bin.

3.2 Simulations

Since these galaxies are so faint, often the reliable host photometry or spectroscopy required to accurately measure physical properties like metallicity and SFR is not available. Therefore it can be useful to use simulations to distinguish between real physical properties, and observational constraints. In Section 3.3, we utilize the IllustrisTNG suite of simulations[5] (Marinacci et al. 2018; Naiman et al. 2018; Nelson et al. 2018, 2019; Pillepich et al. 2018; Springel et al. 2018). IllustrisTNG is a set of large-scale cosmological, gravo-magnetohydrodynamical simulations based on the AREPO code (Springel 2010). We use the TNG100 simulation, which has a volume of 106.5^3 cMpc. This simulation provides the best balance of large haloes (i.e. $M_h > 10^{12}$ $M_\odot$) and smaller resolution subhaloes (i.e. $M_h < 10^9$ $M_\odot$), although qualitatively similar results were found with the use of TNG300. From this simulation, we use stellar masses, SFRs, gas-phase metallicity abundances, galaxy colours, group halo masses, and information about group membership.

3.3 IllustrisTNG

To investigate the tendency of SLSN host-like galaxies to avoid high-density environments further, we make use of the IllustrisTNG suite of simulations. From the TNG100-1 simulation, we obtain stellar masses, gas metallicities, SFRs, and g and i photometry on all 4371 211 subhaloes in the most recent redshift snapshot. Each subhalo resides in a parent halo with a total halo mass M_{200}, defined as the total mass of a sphere whose mean density is 200 times the critical density of the Universe. In line with the properties of SLSN host galaxies, we define a sample of blue low-mass galaxies (BLM),

[5]https://www.tng-project.org/data/

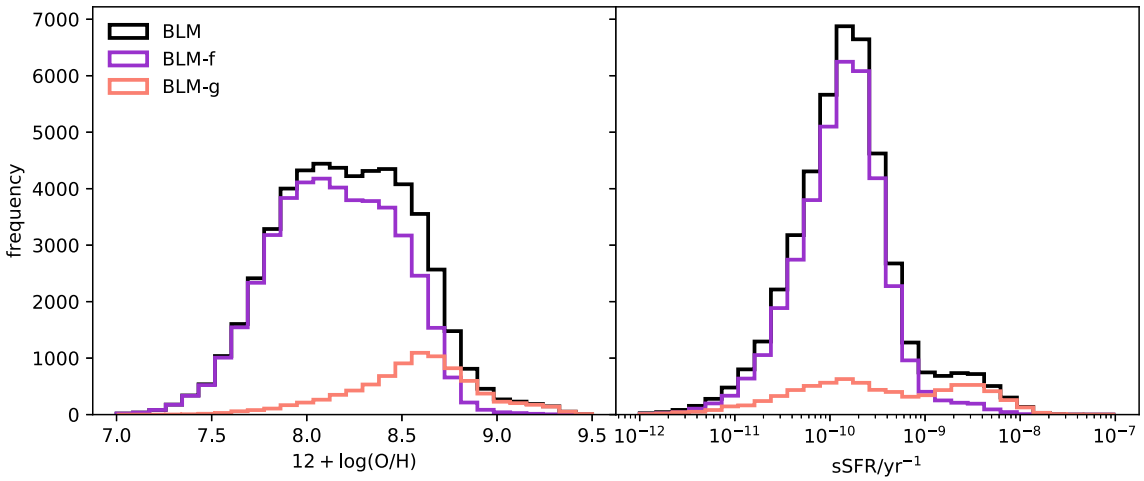

Figure 5. Histograms of metallicity (left) and sSFR (right) in IllustrisTNG for all blue low-mass (BLM) galaxies (black), BLM field galaxies (purple), and BLM group galaxies (orange).

with $(g - i) < 1$ and $10^7 < M_*/\mathrm{M}_\odot < 10^9$. This stellar mass range has an upper limit in line with observations of SLSN host galaxies (e.g. Schulze et al. 2018), and a lower limit to avoid contamination from haloes not yet formed into galaxies. Note that at this stellar mass range, virtually all galaxies (∼98 per cent) have $(g - i) < 1$ and also are star forming. For each subhalo, we retrieve the number of subhaloes (N_{subs}) in its parent halo. For a galaxy to be in a group, we require $N_{\mathrm{subs}} > 1$ and $M_{200} > 10^{12}$ $\mathrm{M}_\odot$. This is to ensure we avoid including field galaxies with smaller (non-galaxy) haloes associated with them. Everything else is assigned as being in the field.

In Fig. 5, we plot a histogram of the log of the metallicity of BLM and a histogram of the log of sSFR, separated by group membership. Immediately it is clear that this sample is biased towards low metallicities, as is expected from observations of SLSN host galaxies (see fig. 11 in Chen et al. 2015, and fig. 8 in Perley et al. 2016b). Notably there are much fewer BLM galaxies in groups than in the field, with group galaxies making up 35.5 per cent of the BLM sample. Additionally, the BLM galaxies that reside in groups lie at the high end of the metallicity distribution. We also see that BLM galaxies typically have intermediate sSFR, as is seen in the properties of SLSN host galaxies. However, BLM galaxies in groups dominate over field galaxies at high sSFR.

Thus, in agreement with our observational results in the previous section, the simulation results qualitatively suggest that the reason SLSN-g are not found in dense environments is because the galaxies that host SLSN, BLM, are not often found in groups. However, quantitatively, there is a potential discrepancy. From the simulation results in Fig. 5 we measure that 35.5 per cent of such BLM galaxies are found in groups within the simulation. This means, observationally, we would expect about 12(235) of SLSN-g(SDSS-m) to be in high-density environments, compared to the 1(4) in SLSN-g(SDSS-m).

This potential discrepancy is pointing to an additional requirement in our simulated sample to properly recover the observed environmental distribution – that of low metallicity. It is known that SLSNe require host galaxies with low metallicities (e.g. Lunnan et al. 2014), and in the simulation results of Fig. 5, the lower metallicity ranges are dominated by field galaxies. We better illustrate this in Fig. 6, where we plot the fractions of field galaxies and group galaxies with respect to the total BLM sample as a function of metallicity. Field galaxies clearly dominate at $Z < \mathrm{Z}_\odot$, and group galaxies dominate at $Z >$

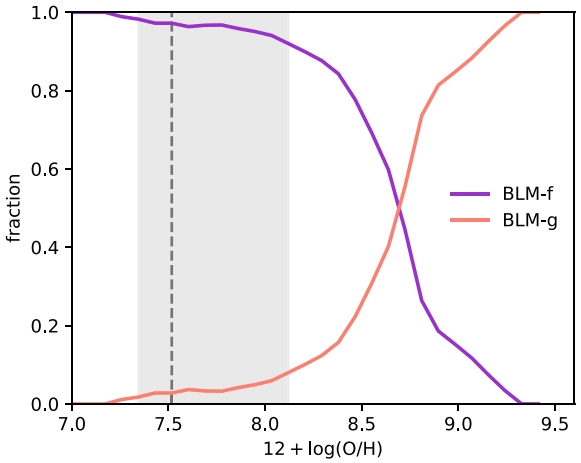

Figure 6. Fractions of BLM-f (purple) and BLM-g (orange) of the total BLM sample with respect to metallicity. The grey dashed line shows the metallicity at which group galaxies account for 3 per cent of the entire BLM sample, in accordance with observations, with upper and lower limits shaded in grey.

$\mathrm{Z}_\odot$; here we assume $\mathrm{Z}_\odot = 8.69$ following Asplund et al. (2009). We also plot the metallicity at which the fraction of observed SLSN host galaxies in groups are 0.03. We can then apply generous constraints by considering the uncertainties on the SLSN occurrence rate above. By computing beta distribution confidence intervals at $c = 0.68$ (Cameron 2011) on the fraction of observed SLSNe in groups, we find this fraction to be $0.03^{+0.09}_{-0.02}$. In Fig. 6 these confidence intervals are shaded in grey. Even with such a wide confidence interval, the highest metallicity that is consistent with the observed environmental density of SLSN hosts, and therefore the apparent upper limit of SLSN production is $12 + \log(\mathrm{O/H}) = 8.12$. This is approximately 0.2 dex lower than the apparent threshold reported in Schulze et al. (2018), $12 + \log(\mathrm{O/H}) \sim 8.3$, and 0.3 dex lower than the threshold reported in Chen et al. (2017), $12 + \log(\mathrm{O/H}) \sim 8.4$.

In addition, we find that only about 26 per cent of BLM galaxies in groups reside in haloes of $M_{\mathrm{h}} \geq 10^{13}$ $\mathrm{M}_\odot$. This supports the idea that the typical galaxies that host SLSNe will rarely be found in large groups or clusters.

The distributions in Fig. 5 provide evidence that low metallicity is the constraining requirement for SLSN production, rather than high

SFR. Focusing on the right-hand panel, we see that the distribution of BLM-g in sSFR is more evenly distributed compared to metallicity in the left-hand panel. In particular, noting SLSN host galaxies require sSFR$\gtrsim 10^{-9}$ yr^{-1} (Schulze et al. 2018), there is actually an excess of BLM-g galaxies at this sSFR. This means that if a high sSFR was the predominant factor for SLSN production compared to low metallicity, we would see many more SLSN host galaxies in denser environments: ≈24 out of the 33 SLSN events in this sample. Since this is not the case, our analysis suggests that low metallicity is likely the more important requirement.

4 CONCLUSIONS

Using SLSN sources from the ZTF BTS, we calculate whether their host galaxies are found in high-density or low-density large-scale environments. We use bright, spectroscopically redshifted galaxies with absolute magnitude $M_i < -21.5$ as tracers of density, and classify a source as in a high-density environment if there are two or more bright galaxies within 2 Mpc. We test our findings by comparing the SLSN sample with a sample of Type Ia SNe, whose host galaxies span a wider range of galaxy colour and absolute magnitude. We also create another sample, derived from SDSS photometrically redshifted galaxies, matched to the SLSN host galaxies in galaxy colour, absolute magnitude, and redshift. Our main findings may be summarized as follows.

(i) SLSN host galaxies are almost always located in low-density environments, with all but two (of 33) host galaxies having no bright galaxies within 2 Mpc. The photometrically selected matched sample (in luminosity, colour, and redshift) shows similar results. This is in contrast to Type Ia SN host galaxies, 8.5 per cent of which have two or more bright neighbours This is consistent with the fraction of SNe Ia found in clusters compared to field galaxies, according to Larison et al. (2023). In any relevant magnitude bin, the maximum high-density fraction is <10 per cent for the SLSN and matched samples, while for the SN-Ia sample the minimum is >20 per cent.

(ii) In analysis of the IllustrisTNG simulations, over 70 per cent of BLM galaxies are found in the field, rather than in groups. These galaxies have low metallicities and high SFRs, which are typical of SLSN host galaxies.

(iii) Crucially, we find that in order to quantitatively match the rate of SLSN host galaxies found in dense environments, an additional condition on the metallicity of the host in the simulation is required. Taking the uncertainties into account, SLSN production is only favoured in galaxies with $12 + \log(\mathrm{O/H}) = 8.12$. In contrast, selecting only high-sSFR galaxies would lead to an overrepresentation of high-density hosts in the simulation.

The fact that simulations suggest that galaxies capable of producing SLSNe and having high sSFR would preferentially be found in groups, but such galaxies with low metallicity would preferentially be found in the field, suggests that the metallicity of a galaxy is the more important factor in the occurrence of these explosive transients. However, this result will be strengthened with more observations of SLSNe and their host galaxies, which will be achieved over the coming years when new high-cadence surveys come online such as the Vera C. Rubin Observatory.

ACKNOWLEDGEMENTS

The authors thank the anonymous reviewer for their helpful and thoughtful comments on this paper. CC acknowledges support from the School of Physics and Astronomy at the University of Birmingham. SLM acknowledges support from STFC grant no. ST/S000305/1 and UK Space Agency grants nos ST/Y000692/1 and ST/X002071/1. MN is supported by the European Research Council (ERC) under the European Union's Horizon 2020 Framework Programme (grant agreement no. 948381).

Funding for the Sloan Digital Sky Survey IV has been provided by the Alfred P. Sloan Foundation, the U.S. Department of Energy Office of Science, and the Participating Institutions.

SDSS-IV acknowledges support and resources from the Center for High Performance Computing at the University of Utah. The SDSS website is www.sdss.org.

SDSS-IV is managed by the Astrophysical Research Consortium for the Participating Institutions of the SDSS Collaboration including the Brazilian Participation Group, the Carnegie Institution for Science, Carnegie Mellon University, Center for Astrophysics| Harvard & Smithsonian, the Chilean Participation Group, the French Participation Group, Instituto de Astrofísica de Canarias, The Johns Hopkins University, Kavli Institute for the Physics and Mathematics of the Universe (IPMU)/University of Tokyo, the Korean Participation Group, Lawrence Berkeley National Laboratory, Leibniz Institut für Astrophysik Potsdam (AIP), Max-Planck-Institut für Astronomie (MPIA Heidelberg), Max-Planck-Institut für Astrophysik (MPA Garching), Max-Planck-Institut für Extraterrestrische Physik (MPE), National Astronomical Observatories of China, New Mexico State University, New York University, University of Notre Dame, Observatário Nacional/MCTI, The Ohio State University, Pennsylvania State University, Shanghai Astronomical Observatory, United Kingdom Participation Group, Universidad Nacional Autónoma de México, University of Arizona, University of Colorado Boulder, University of Oxford, University of Portsmouth, University of Utah, University of Virginia, University of Washington, University of Wisconsin, Vanderbilt University, and Yale University.

This study is based on observations obtained with the 48-inch Samuel Oschin telescope and the 60-inch telescope at the Palomar Observatory as part of the Zwicky Transient Facility (ZTF) project. ZTF is supported by the National Science Foundation under grant nos AST-1440341 and AST-2034437, and a collaboration including current partners Caltech, IPAC, the Weizmann Institute for Science, the Oskar Klein Center at Stockholm University, the University of Maryland, Deutsches Elektronen-Synchrotron and Humboldt University, the TANGO Consortium of Taiwan, the University of Wisconsin at Milwaukee, Trinity College Dublin, Lawrence Livermore National Laboratories, IN2P3, University of Warwick, Ruhr University Bochum, Northwestern University and former partners the University of Washington, Los Alamos National Laboratories, and Lawrence Berkeley National Laboratories. Operations are conducted by COO, IPAC, and UW.

The IllustrisTNG simulations were undertaken with compute time awarded by the Gauss Centre for Supercomputing (GCS) under GCS Large-Scale Projects GCS-ILLU and GCS-DWAR on the GCS share of the supercomputer Hazel Hen at the High Performance Computing Center Stuttgart (HLRS), as well as on the machines of the Max Planck Computing and Data Facility (MPCDF) in Garching, Germany.

DATA AVAILABILITY

The data used for this analysis are available at the links in the text above where the data are described.

REFERENCES

Abdurro'uf et al., 2022, ApJS, 259, 35
Angus C. R., Levan A. J., Perley D. A., Tanvir N. R., Lyman J. D., Stanway E. R., Fruchter A. S., 2016, MNRAS, 458, 84
Angus C. R. et al., 2019, MNRAS, 487, 2215
Asplund M., Grevesse N., Sauval A. J., Scott P., 2009, ARA&A, 47, 481
Ayala B., Gutierrez C., Kravtsov T., Yaron O., 2022, Transient Name Server Classification Rep., 2022-2393, 1
Bellm E. C. et al., 2019, PASP, 131, 018002
Blanchard P., Gomez S., Hosseinzadeh G., Berger E., 2020, Transient Name Server Classification Rep., 2020-3871, 1
Blanton M. R. et al., 2017, AJ, 154, 28
Cameron E., 2011, Publ. Astron. Soc. Aust., 28, 128
Chambers K. C. et al., 2016, preprint (arXiv:1612.05560)
Chatzopoulos E., Wheeler J. C., Vinko J., 2012, ApJ, 746, 121
Chen T., 2019, Transient Name Server Classification Rep., 2019-938, 1
Chen T.-W. et al., 2013, ApJ, 763, L28
Chen T. W. et al., 2015, MNRAS, 452, 1567
Chen T.-W., Smartt S. J., Yates R. M., Nicholl M., Krühler T., Schady P., Dennefeld M., Inserra C., 2017, MNRAS, 470, 3566
Chevalier R. A., Irwin C. M., 2011, ApJ, 729, L6
Cleland C., McGee S. L., 2021, MNRAS, 500, 590
Cooper M. C., Newman J. A., Yan R., 2009, ApJ, 704, 687
Dahiwale A., Fremling C., 2020, Transient Name Server Classification Rep., 2020-1756, 1
Dahiwale A., Fremling C., 2021, Transient Name Server Classification Rep., 2021-1234, 1
Davis K., Foley R., Dimitriadis G., Soto K. D., 2022, Transient Name Server Classification Rep., 2022-1881, 1
Deckers M., Prentice S., Maguire K., Dimitriadis G., Magee M., Harvey L., Terwel J., 2021, Transient Name Server Classification Rep., 2021-1365, 1
Doi M. et al., 2010, AJ, 139, 1628
Dong S., 2018, Transient Name Server Classification Rep., 2018-673, 1
Dressler A., 1980, ApJ, 236, 351
Ellison S. L., Simard L., Cowan N. B., Baldry I. K., Patton D. R., McConnachie A. W., 2009, MNRAS, 396, 1257
Flewelling H. A. et al., 2020, ApJS, 251, 7
Fremling C., Dahiwale A., 2019, Transient Name Server Classification Rep., 2019-1774, 1
Fremling C., Sharma Y., 2018, Transient Name Server Classification Rep., 2018-815, 1
Fremling C., Dugas A., Sharma Y., 2018a, Transient Name Server Classification Rep., 2018-1232, 1
Fremling C., Dugas A., Sharma Y., 2018b, Transient Name Server Classification Rep., 2018-1411, 1
Fremling C., Dugas A., Sharma Y., 2018c, Transient Name Server Classification Rep., 2018-1416, 1
Fremling C., Dugas A., Sharma Y., 2018d, Transient Name Server Classification Rep., 2018-1870, 1
Fremling C., Dugas A., Sharma Y., 2018e, Transient Name Server Classification Rep., 2018-1877, 1
Fremling C., Dugas A., Sharma Y., 2019a, Transient Name Server Classification Rep., 2019-32, 1
Fremling C., Dugas A., Sharma Y., 2019b, Transient Name Server Classification Rep., 2019-188, 1
Fremling C., Dugas A., Sharma Y., 2019c, Transient Name Server Classification Rep., 2019-598, 1
Fremling C., Dugas A., Sharma Y., 2019d, Transient Name Server Classification Rep., 2019-636, 1
Fremling C., Dugas A., Sharma Y., 2019e, Transient Name Server Classification Rep., 2019-747, 1
Fremling C., Dugas A., Sharma Y., 2019f, Transient Name Server Classification Rep., 2019-952, 1
Fremling C., Sharma Y., Dahiwale A., 2019g, Transient Name Server Classification Rep., 2019-1838, 1
Fremling C., Dahiwale A., Dugas A., 2019h, Transient Name Server Classification Rep., 2019-1923, 1
Fukugita M., Ichikawa T., Gunn J. E., Doi M., Shimasaku K., Schneider D. P., 1996, AJ, 111, 1748
Gal-Yam A., 2012, Science, 337, 927
Gillanders J., Srivastav S., Fulton M., Shingles L. J., Smith K. W., Zimmerman E., 2021, Transient Name Server Classification Rep., 2021-86, 1
Ginzburg S., Balberg S., 2012, ApJ, 757, 178
Gomez S., Hosseinzadeh G., Berger E., Blanchard P., 2021a, Transient Name Server Classification Rep., 2021-565, 1
Gomez S., Hosseinzadeh G., Berger E., Blanchard P., 2021b, Transient Name Server Classification Rep., 2021-3270, 1
Gomez S., Hosseinzadeh G., Blanchard P., Berger E., 2021c, Transient Name Server Classification Rep., 2021-3662, 1
Gonzalez E. P., Hiramatsu D., Burke J., Howell D. A., McCully C., Pellegrino C., 2021, Transient Name Server Classification Rep., 2021-1220, 1
Gromadzki M., Wevers T., Lyman J., Yaron O., 2018, Transient Name Server Classification Rep., 2018-1396, 1
Gromadzki M., Cartier R., Yaron O., 2021, Transient Name Server Classification Rep., 2021-3651, 1
Gunn J. E. et al., 1998, AJ, 116, 3040
Gunn J. E. et al., 2006, AJ, 131, 2332
Harvey L., Deckers M., Dimitriadis G., Burgaz U., Yaron O., 2022, Transient Name Server Classification Rep., 2022-2997, 1
Ihanec N., Gromadzki M., Wevers T., Irani I., 2020, Transient Name Server Classification Rep., 2020-3486, 1
Inserra C. et al., 2013, ApJ, 770, 128
Kasen D., Bildsten L., 2010, ApJ, 717, 245
Larison C., Jha S., Kwok L., Camacho-Neves Y., 2023, preprint (arXiv:2306.01088)
Leloudas G. et al., 2015, MNRAS, 449, 917
Lunnan R. et al., 2014, ApJ, 787, 138
Lunnan R. et al., 2018, ApJ, 852, 81
Magee M., Terwel J., Prentice S., Harvey L., Strotjohann N. L., 2021, Transient Name Server Classification Rep., 2021-338, 1
Marinacci F. et al., 2018, MNRAS, 480, 5113
Masci F. J. et al., 2019, PASP, 131, 018003
Naiman J. P. et al., 2018, MNRAS, 477, 1206
Neill J. D. et al., 2011, ApJ, 727, 15
Nelson D. et al., 2018, MNRAS, 475, 624
Nelson D. et al., 2019, Comput. Astrophys. Cosmol., 6, 2
Nicholl M., Guillochon J., Berger E., 2017, ApJ, 850, 55
Nicholl M., Short P., Lawrence A., Ross N., Smartt S., Oates S., 2019, Transient Name Server Classification Rep., 2019-2271, 1
Ørum S. V., Ivens D. L., Strandberg P., Leloudas G., Man A. W. S., Schulze S., 2020, A&A, 643, A47
Perez-Fournon I. et al., 2020, Transient Name Server Classification Rep., 2020-2456, 1
Perley D. A., 2019, Transient Name Server Classification Rep., 2019-1646, 1
Perley D. A. et al., 2016a, ApJ, 817, 8
Perley D. A. et al., 2016b, ApJ, 830, 13
Perley D., Yan L., Andreoni I., Karambelkar V., Sharma Y., De K., Fremling C., Kulkarni S., 2019, Transient Name Server Classification Rep., 2019-1712, 1
Perley D. A. et al., 2020a, ApJ, 904, 35
Perley D. A., Taggart K., Dahiwale A., Fremling C., 2020b, Transient Name Server Classification Rep., 2020-1749, 1
Perley D., Sollerman J., Fremling C., Dahiwale A., Walters R., 2020c, Transient Name Server Classification Rep., 2020-3125, 1
Perley D. A., Yao Y., Chen T., Schulze S., Sharma Y., Ho A. Y. Q., Yan L., Kulkarni S. R., 2021, Transient Name Server Classification Rep., 2021-1649, 1
Pillepich A. et al., 2018, MNRAS, 475, 648
Poidevin F. et al., 2020, Transient Name Server Classification Rep., 2020-500, 1
Poidevin F. et al., 2021, Transient Name Server Classification Rep., 2021-2271, 1

Poidevin F. et al., 2022, Transient Name Server Classification Rep., 2022-1175, 1
Prentice S. J., Maguire K., Skillen K., Magee M. R., Clark P., 2019a, Transient Name Server Classification Rep., 2019-1598, 1
Prentice S. J., Maguire K., Skillen K., Magee M. R., Clark P., 2019b, Transient Name Server Classification Rep., 2019-2339, 1
Quimby R. M. et al., 2011, Nature, 474, 487
Quimby R. M. et al., 2018, ApJ, 855, 2
Schulze S. et al., 2018, MNRAS, 473, 1258
Smee S. A. et al., 2013, AJ, 146, 32
Smith N., McCray R., 2007, ApJ, 671, L17
Smith M. et al., 2012, ApJ, 755, 61
Smith K. W. et al., 2019, Res. Notes Am. Astron. Soc., 3, 26
Smith K. W. et al., 2020, PASP, 132, 085002
Smith K. W., Fulton M., Moore T., Srivastav S., Yaron O., 2022, Transient Name Server Classification Rep., 2022-583, 1
Springel V., 2010, MNRAS, 401, 791
Springel V. et al., 2018, MNRAS, 475, 676
Srivastav S., Fulton M., Moore T., Yaron O., 2022, Transient Name Server Classification Rep., 2022-667, 1
Sullivan M. et al., 2006, ApJ, 648, 868
Terreran G., 2020, Transient Name Server Classification Rep., 2020-2902, 1
Tonry J. L. et al., 2018, PASP, 130, 064505
Tremonti C. A. et al., 2004, ApJ, 613, 898
Weil K. E., Subrayan B. M., Milisavljevic D., 2021, Transient Name Server Classification Rep., 2021-2270, 1
Wetzel A. R., Tinker J. L., Conroy C., van den Bosch F. C., 2013, MNRAS, 432, 336
Wiseman P. et al., 2021, MNRAS, 506, 3330
Yan L., Perley D., Schulze S., Cook D., Chen T. W., Gal-Yam A., Lunnan R., Taggart K., 2020a, Transient Name Server Classification Rep., 2020-1736, 1
Yan L., Perley D., Schulze S., Andreoni I., Dahiwale A., Gal-Yam A., Lunnan R., Taggart K., 2020b, Transient Name Server Classification Rep., 2020-1737, 1
Yang X., Mo H. J., van den Bosch F. C., Pasquali A., Li C., Barden M., 2007, ApJ, 671, 153
Yao Y., Velzen S. V., Tzanidakis A., Gezari S., Hammerstein E., Somalwar J., Kulkarni S., 2021, Transient Name Server Classification Rep., 2021-1614, 1

APPENDIX A:

Table A1 lists all 55 SLSNe events that were available on the BTS when analysis began, the groups that classified them as SLSNe, and the relevant citation.

Table A1. ZTF IDs of the transient events that were obtained on the BTS, the group that classified them as SLSNe, and the relevant citation.

ZTF ID	Classifying group	Citation
ZTF18aavrmcg	NUTS	Dong (2018)
ZTF18aapgrxo	ZTF	Fremling & Sharma (2018)
ZTF18abmasep	ZTF	Fremling, Dugas & Sharma (2018a)
ZTF18ablwafp	ePESSTO	Gromadzki et al. (2018)
ZTF18abshezu	ZTF	Fremling, Dugas & Sharma (2018b)
ZTF18abvgjyl	ZTF	Fremling, Dugas & Sharma (2018c)
ZTF18acapyww	ZTF	Fremling, Dugas & Sharma (2018d)
ZTF18acenqto	ZTF	Fremling, Dugas & Sharma (2018e)
ZTF18achdidy	ZTF	Fremling, Dugas & Sharma (2019a)
ZTF18acxgqxq	ZTF	Fremling et al. (2019a)
ZTF18acyxnyw	ZTF	Fremling, Dugas & Sharma (2019b)
ZTF19aaknqmp	ZTF	Fremling, Dugas & Sharma (2019c)
ZTF19aanesgt	ZTF	Fremling, Dugas & Sharma (2019d)
ZTF19aacxrab	ZTF	Fremling, Dugas & Sharma (2019e)
ZTF19aavouyw	None	Chen (2019)
ZTF19aarphwc	ZTF	Fremling, Dugas & Sharma (2019f)
ZTF19aawfbtg	TCD	Prentice et al. (2019a)
ZTF19abpbopt	ZTF	Perley (2019)
ZTF19abnacvf	ZTF	Perley et al. (2019)
ZTF19abfvnns	ZTF	Fremling & Dahiwale (2019)
ZTF18aajqcue	ZTF	Fremling, Sharma & Dahiwale (2019g)
ZTF19abxgmzr	ZTF	Fremling, Dahiwale & Dugas (2019h)
ZTF19acfwynw	C-SNAILS	Nicholl et al. (2019)
ZTF19acgjpgh	TCD	Prentice et al. (2019b)
ZTF20aahbfmf	SGLF	Poidevin et al. (2020)
ZTF20aaifybu	ZTF	Yan et al. (2020a)
ZTF19acbonaa	ZTF	Yan et al. (2020b)
ZTF20aayprqz	ZTF	Perley et al. (2020b)
ZTF20aattyuz	ZTF	Dahiwale & Fremling (2020)
ZTF20abobpcb	SGLF	Perez-Fournon et al. (2020)
ZTF20abpuwxl	None	Terreran (2020)
ZTF20abzumlr	ZTF	Perley et al. (2020c)
ZTF20acphdcg	ePESSTO+	Ihanec et al. (2020)
ZTF20acpyldh	FLEET	Blanchard et al. (2020)
ZTF21aaarmti	ePESSTO+	Gillanders et al. (2021)
ZTF21aagpymw	ePESSTO+	Magee et al. (2021)
ZTF19ackjrru	FLEET	Gomez et al. (2021a)
ZTF19acyjzbe	FLEET	Gomez et al. (2021a)
ZTF19adaivcf	FLEET	Gomez et al. (2021a)
ZTF21aappdnv	Global SN Project	Gonzalez et al. (2021)
ZTF21aakjkec	ZTF	Dahiwale & Fremling (2021)
ZTF21aaxwpyv	TCD	Deckers et al. (2021)
ZTF21aavdqgf	None	Yao et al. (2021)
ZTF21abaiono	ZTF	Perley et al. (2021)
ZTF21abcpsjy	REFITT	Weil, Subrayan & Milisavljevic (2021)
ZTF21abbqeea	SGLF	Poidevin et al. (2021)
ZTF21absyjff	FLEET	Gomez et al. (2021b)
ZTF21accwovq	ePESSTO+	Gromadzki, Cartier & Yaron (2021)
ZTF21abrqria	FLEET	Gomez et al. (2021c)
ZTF21aalkhot	ePESSTO+	Smith et al. (2022)
ZTF22aabimec	ePESSTO+	Srivastav et al. (2022)
ZTF22aadqgoa	SGLF	Poidevin et al. (2022)
ZTF22aalzjdc	UCSC	Davis et al. (2022)
ZTF22aarqrxf	ePESSTO+	Ayala et al. (2022)
ZTF22abcvfgs	ePESSTO+	Harvey et al. (2022)

This paper has been typeset from a TEX/LATEX file prepared by the author.